Circulating heparin oligosaccharides rapidly target the hippocampus in sepsis, potentially impacting cognitive functions

Xing Zhang[a,b,1], Xiaorui Han[a,1], Ke Xia[a], Yongmei Xu[c], Yimu Yang[d], Kaori Oshima[d], Sarah M. Haeger[d], Mario J. Perez[d], Sarah A. McMurtry[d], Joseph A. Hippensteel[d], Joshay A. Ford[d], Paco S. Herson[e], Jian Liu[c], Eric P. Schmidt[d,f], and Robert J. Linhardt[a,g,h,i,2]

[a]Department of Chemistry and Chemical Biology, Rensselaer Polytechnic Institute, Troy, NY 12180; [b]School of Food Science and Pharmaceutical Engineering, Nanjing Normal University, Nanjing 210023, China; [c]Department of Chemical Biology and Medicinal Chemistry, University of North Carolina Eshelman School of Pharmacy, University of North Carolina at Chapel Hill, Chapel Hill, NC 27599; [d]Department of Medicine, University of Colorado Denver, Aurora, CO 80045; [e]Department of Anesthesiology, University of Colorado Denver, Aurora, CO 80045; [f]Department of Medicine, Denver Health Medical Center, Denver, CO 80204; [g]Department of Chemical and Biological Engineering, Rensselaer Polytechnic Institute, Troy, NY 12180; [h]Department of Biomedical Engineering, Rensselaer Polytechnic Institute, Troy, NY 12180; and [i]Center for Biotechnology and Interdisciplinary Studies, Rensselaer Polytechnic Institute, Troy, NY 12180

Edited by Robert Langer, Massachusetts Institute of Technology, Cambridge, MA, and approved March 26, 2019 (received for review February 6, 2019)

Sepsis induces heparanase-mediated degradation of the endothelial glycocalyx, a heparan sulfate-enriched endovascular layer critical to vascular homeostasis, releasing highly sulfated domains of heparan sulfate into the circulation. These domains are oligosaccharides rich in heparin-like trisulfated disaccharide repeating units. Using a chemoenzymatic approach, an undecasaccharide containing a uniformly ^{13}C-labeled internal 2-sulfoiduronic acid residue was synthesized on a *p*-nitrophenylglucuronide acceptor. Selective periodate cleavage afforded a heparin nonasaccharide having a natural structure. This ^{13}C-labeled nonasaccharide was intravenously administered to septic (induced by cecal ligation and puncture, a model of polymicrobial peritonitis-induced sepsis) and nonseptic (sham) mice. Selected tissues and biological fluids from the mice were harvested at various time points over 4 hours, and the ^{13}C-labeled nonasaccharide was recovered and digested with heparin lyases. The resulting ^{13}C-labeled trisulfated disaccharide was quantified, without interference from endogenous mouse heparan sulfate/heparin, using liquid chromatography–mass spectrometry with sensitive and selective multiple reaction monitoring. The ^{13}C-labeled heparin nonasaccharide appeared immediately in the blood and was rapidly cleared through the urine. Plasma nonasaccharide clearance was only slightly prolonged in septic mice ($t_{1/2}$ ~ 90 minutes). In septic mice, the nonasaccharide penetrated into the hippocampus but not the cortex of the brain; no hippocampal or cortical brain penetration occurred in sham mice. The results of this study suggest that circulating heparan sulfates are rapidly cleared from the plasma during sepsis and selectively penetrate the hippocampus, where they may have functional consequences.

heparin oligosaccharides | sepsis | distribution | brain | stable isotope labeling

Sepsis, the injurious systemic response to infection, is the most common cause of in-hospital death in the United States (1). Patients fortunate enough to survive sepsis frequently experience long-term morbidity, such as persistent cognitive impairment (2). Emerging evidence has indicated that sepsis-induced degradation of the endothelial glycocalyx, a heparan sulfate-rich endovascular layer, mediates the onset of organ injury during sepsis, leading to patient morbidity and mortality (3–5). Heparan sulfates are the glycan side chains of proteoglycans, including syndecans and glypicans (6). There is accordingly a need to detect ongoing glycocalyx degradation in septic patients, as this may predict patient outcomes and guide clinical decision making (7).

The bedside detection of glycocalyx degradation during sepsis (mediated by "sheddases" such as heparanase, a mammalian endoglucuronidase acting on heparan sulfate) has been largely performed by measuring glycocalyx breakdown products (e.g., highly sulfated, heparin-like, heparan sulfate fragments, approximately octasaccharide to decasaccharide in size) in the plasma of septic patients (4). However, as heparan sulfate fragments can persist in the plasma for up to 7 d after sepsis onset (4, 8), it is uncertain whether the persistence of circulating heparan sulfate fragments reflects ongoing glycocalyx degradation or rather sepsis-associated impairment in the endogenous processes of plasma heparan sulfate clearance. For circulating heparan sulfate fragments to retain their value as biomarkers of ongoing glycocalyx injury, it is necessary to determine the half-life of circulating heparan sulfate in a septic host.

We have recently demonstrated that sepsis induces accumulation of circulating, highly sulfated heparan sulfate fragments within the hippocampus, a region of the brain implicated in memory formation (8). In both mice and humans, hippocampal-penetrating heparan sulfate was of sufficient size and sulfation to sequester and inhibit the activity of brain-derived neurotrophic factor (BDNF), a

Significance

Sepsis results in the heparanase-mediated release of heparan sulfate oligosaccharides from the endothelial glycocalyx. In human sepsis patients, these released heparan sulfate oligosaccharides have been shown to be rich in highly sulfated domains, and their presence was associated with moderate or severe cognitive impairment. The current study uses a murine sepsis model to show that an exogenously administered highly sulfated ^{13}C-labeled heparan sulfate oligosaccharide, rich in highly sulfated domains, selectively targets the hippocampus. This selective targeting suggests that heparan sulfate sequestering of brain-derived neurotrophic factor in the hippocampus may impact spatial memory formation. A therapeutic strategy for selectively protecting cognition in septic patients might be developed through targeting these heparan sulfate oligosaccharides, rich in highly sulfated domains.

Author contributions: J.L., E.P.S., and R.J.L. designed research; X.Z., X.H., Y.X., Y.Y., K.O., S.M.H., M.J.P., S.A.M., J.A.H., J.A.F., and P.S.H. performed research; K.X., J.L., E.P.S., and R.J.L. analyzed data; and J.L., E.P.S., and R.J.L. wrote the paper.

The authors declare no conflict of interest.

This article is a PNAS Direct Submission.

[1]X.Z. and X.H. contributed equally to this work.

[2]To whom correspondence should be addressed. Email: linhar@rpi.edu.

This article contains supporting information online at www.pnas.org/lookup/suppl/doi:10.1073/pnas.1902227116/-/DCSupplemental.

Published online April 22, 2019.

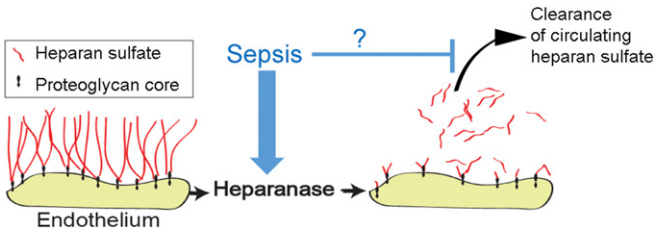

Fig. 1. Overall hypothesis. Septic induction of endothelial heparanase degrades heparan sulfate from the endothelial glycocalyx, causing both local vascular injury as well as releasing highly sulfated, heparin-like heparan sulfate oligosaccharides into the plasma. We hypothesized that sepsis not only induces heparan sulfate fragmentation but also impedes clearance of these fragments, leading to persistence of circulating heparan sulfate oligosaccharides in septic patients.

growth factor necessary for spatial memory formation. Accordingly, the presence of circulating heparan sulfate in septic patients predicts persistent impairments in cognitive function (8). The degree to which circulating heparan sulfate selectively penetrates the hippocampus in comparison with other neuronal (brain cortex) and non-neuronal (e.g., lung, fat, liver, kidney, etc.) tissues remains unknown.

For this study, we hypothesized that circulating heparan sulfate oligosaccharides rapidly clear from the circulation in healthy, nonseptic animals. Furthermore, we hypothesized that sepsis impairs this rapid clearance of circulating heparan sulfate, prolonging the opportunity for penetration of circulating heparan sulfate into tissues. Last, we hypothesized that this penetration was particularly evident in the hippocampus, compared with other tissues, thus contributing to the long-term neurological consequences of sepsis (Fig. 1).

Heparan sulfate is composed of a linear, repeating disaccharide unit of sulfated uronic acids [D-glucuronic acid (GlcA) and L-iduronic acid (IdoA)] and D-glucosamine (GlcN) residues, →4) GlcA/IdoA (±2S) (1 → 4) Glc(NAc/S) (±3S,6S) (1→, where S is sulfo and Ac is acetyl) (9). Heparin is a closely related, anticoagulant polysaccharide, a more highly sulfated version of heparan sulfate, composed primarily of the Tri-S repeating unit →4) IdoA2S (1 → 4) GlcNS6S (1→ (9). Heparan sulfate contains long domains with no (or low) sulfation →4) GlcA (1 → 4) GlcNAc, at which heparanase acts, and shorter, heparanase-resistant, heparin-like Tri-S domains (10).

Results

Synthesis of ^{13}C-Labeled Heparin Oligosaccharide. Based on our previous efforts in preparing homogeneous low–molecular-weight heparins (11–13), the chemoenzymatic synthesis of a natural-like ^{13}C-labeled heparin nonasaccharide **11** rich in Tri-S repeating units flanked by two GlcA residues was initiated from the commercially available *p*-nitrophenyl glucuronide (GlcA-*p*NP) (**1**) (Fig. 2*A*). The monosaccharide acceptor **1** was repetitively elongated with heparosan synthase 2 from *Pasteurella multocida* (PmHS2), UDP-*N*-trifluoroacetyl glucosamine (GlcNTFA) donor, and UDP-glucuronic acid (GlcA) to form hexasaccharide **2**. Selective removal of the trifluoroacetic acid (TFA) group from the GlcN nitrogen, followed by *N*-sulfonation, C_5-epimerization/2-sulfation, and chain elongations produced octasaccharide **5**. UDP-[^{13}C]GlcA was subsequently used to introduce ^{13}C-labeled GlcA residue, which after a series of repetitive steps followed 6-sulfation, the key undecasaccharide intermediate **9**, containing an internal [^{13}C]IdoA2S residue, was prepared for further degradation. During this chemoenzymatic synthesis, the strong UV absorbance and high C-18 binding affinity of the *p*-NP group facilitates the detection and purification of the intermediates (11–13).

Treatment of compound **9** with periodate oxidation followed by a modified alkaline degradation resulted in the selective cleavage of vicinal diols (14), in the two flanking GlcA residues, affording compound **10** (Fig. 2*B*). Subsequent acidic hydrolysis, using 0.5 M TFA, removed the aglycone (14) to obtain the Tri-S–rich heparin nonasaccharide **11** having a completely natural structure

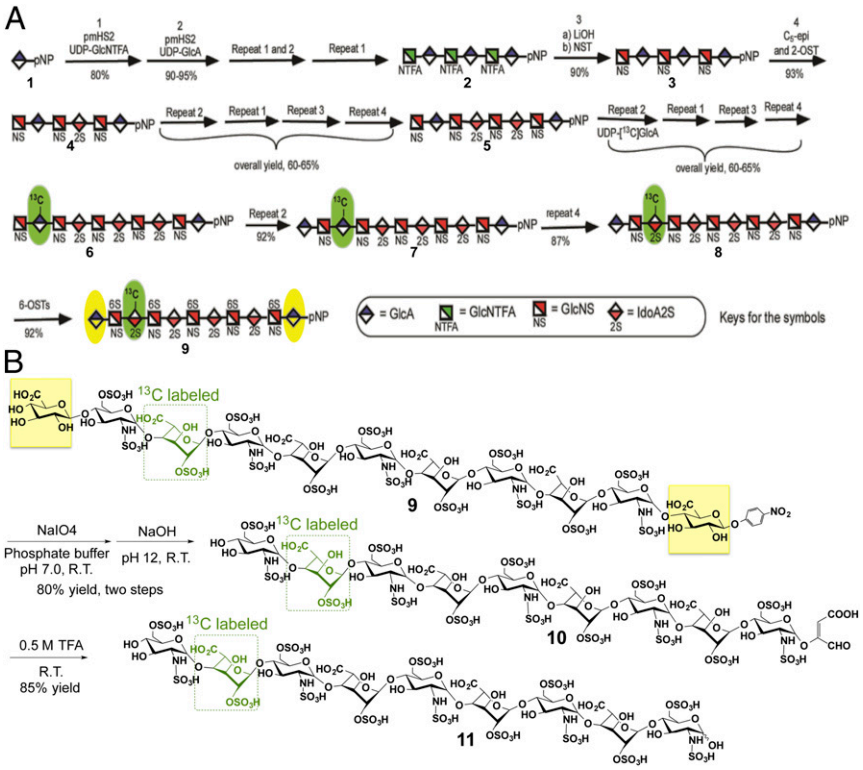

Fig. 2. Scheme is shown for the synthesis of ^{13}C-labeled oligosaccharides **9** and **11**. *A* uses symbolic structures to show the chemoenzymatic synthesis of the key intermediate **9**. The [^{13}C]IdoA2S residue is highlighted in green, and the flanking GlcA residues are highlighted in yellow. *B* uses chemical structures to show the cleavage of undecasaccharide **9** at its flanking GlcA residues and the formation of nonasaccharide **11** composed of Tri-S disaccharide repeating units containing an internal [^{13}C]IdoA2S residue (green).

(except for a ^{13}C-labeled IdoA2S residue) found in heparin and in the heparanase-resistant domains of heparan sulfate.

Characterization of ^{13}C-Labeled Heparin Oligosaccharides. The structure of the final oligosaccharide **11** is supported by liquid chromatography–mass spectrometry (LC-MS) and 1D- and 2D-NMR spectroscopy (Fig. 3). Comparison of the ^{1}H-NMR spectra of undecasaccharide **9** and nonasaccharide **11** showed the disappearance of the C1 signals at 4.52 and 5.23 ppm associated with the two GlcA residues in compound **11**, demonstrating that they had been oxidatively removed (Fig. 3 *A* and *B*). The remaining anomeric signals, at 5.34 and 5.14 ppm, confirmed the presence of only the respective GlcNS6S and IdoA2S residues in **11** (Fig. 3*A*). The significantly stronger signals of one IdoA residue in 2D-^{1}H-^{13}C–heteronuclear single-quantum coherence (HSQC) spectrum confirmed presence of the [^{13}C]IdoA2S residue (Fig. 3*D*). The H–H COSY spectrum of **11** provided the assignments of the H-2, H-4, and H-5 of the IdoA residues to peaks at 4.26, 4.02, and 4.76 ppm, respectively, confirming that all contained 2-*O*-sulfo groups (Fig. 3*C*). The total proton assignments for compounds **9** and **11** are provided in *SI Appendix*, Tables S1 and S2. The structure was also characterized by high-resolution LC-MS of compound **11** afforded an *m*/*z* of 622.2147 in negative mode, corresponding to $[M–4H]^{4–}$ (*SI Appendix*, Fig. S1), and the purity of **11** was assessed to be >99% based on LC and polyacrylamide gel electrophoresis (PAGE) (*SI Appendix*, Fig. S2).

Administration of ^{13}C-Labeled Heparin Oligosaccharide in Normal and Septic Mice. Twenty-four hours after cecal ligation and puncture (CLP) (n = 11) or sham (n = 9), we administered 15 μg (in 100 μL of saline) of pure nonasaccharide **11** to individual mice by tail vein injection. The 24-h time point was chosen as this was the point of maximal septic glycocalyx degradation, at which peak circulating heparan sulfate occurs (15). As demonstrated in Fig. 4, at least three animals from both the CLP and sham groups were killed 30, 120, and 240 min after nonasaccharide injection, and biological fluids and selected organs were collected. A third control group (n = 3) did not undergo surgery, were not administered nonasaccharide, and were killed for tissue collection.

Analysis of the Distribution of ^{13}C-Labeled Heparin Oligosaccharides. Tissue samples were defatted and then proteolyzed to recover all of their sulfated oligosaccharides and polysaccharides; these would include both endogenous (unlabeled) heparan sulfate and the exogenously administered ^{13}C-labeled nonasaccharide **11**. The purified sulfated oligosaccharides and polysaccharides were treated with polysaccharide lyases to completely digest these into their constituent disaccharides for LC-MS analysis (Fig. 5*A*). These include eight different unlabeled disaccharides afforded on digestion of the endogenous heparan sulfate and three unlabeled Tri-S disaccharides and one ^{13}C-labeled Tri-S disaccharide from nonasaccharide **11**. The ^{13}C-labeled Tri-S disaccharide was separated by MS based on its 6-amu difference from the unlabeled Tri-S disaccharide (arising from both **11** and endogenous heparan sulfate). LC-MS relying on sensitive and selective multiple-reaction monitoring (MRM) (16) was used to quantify ^{13}C-labeled Tri-S disaccharide and, thus, the content of **11** in each tissue (see *SI Appendix* for experiment details).

Average sample recoveries of ∼45% and ∼69% from brain tissue and plasma, respectively, were determined using different amounts of pure ^{13}C-labeled nonasaccharide **11**. This recovery was linear over the range of 0.01–600 ng in 5 μL of plasma sample (*SI Appendix*, Fig. S3 and Table S3). ^{13}C-labeled Tri-S disaccharide standard was used to determine a limit of detection (LOD) of 5 pg per injection (2-μL injection volume) and limit of quantification (LOQ) of 17 pg (2-μL injection volume) for each disaccharide produced on heparin lyase treatment (17), corresponding to an LOD for nonasaccharide of 20 pg and LOQ of 70 pg. The sensitivity of analysis was sufficient to analyze ^{13}C-labeled nonasaccharide **11** in biological fluids or organs in the mouse in which it was retained or concentrated. Thus, MRM analysis facilitates the sensitive and selective detection of picogram amounts of exogenously administered ^{13}C-heparan sulfate/heparin oligosaccharide, in tissues such as mouse brain, even in the

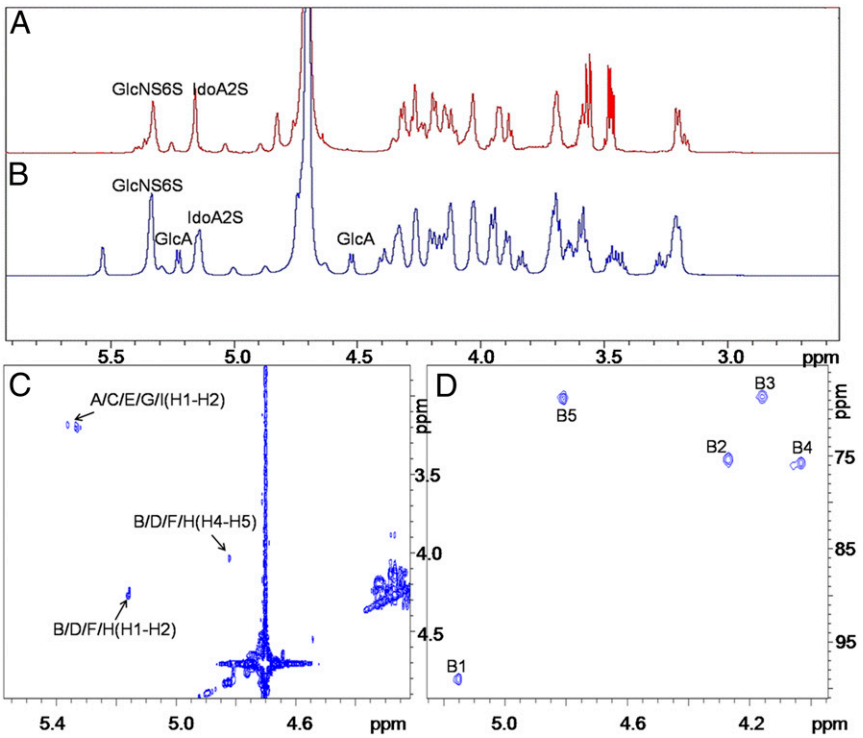

Fig. 3. NMR is used for the characterization of key intermediate **9** and final oligosaccharide **11**. *A* and *B* show the 1D-^{1}H NMR spectra of compounds **11** and **9**, respectively, with anomeric signals identified. *C* and *D* show the 2D COSY and HSQC spectra, respectively, of compound **11**. The cross-peaks are labeled based on the structure in Fig. 2*B*. The letters in *C* and *D* correspond to those in the assignment table (*SI Appendix*, Table S2).

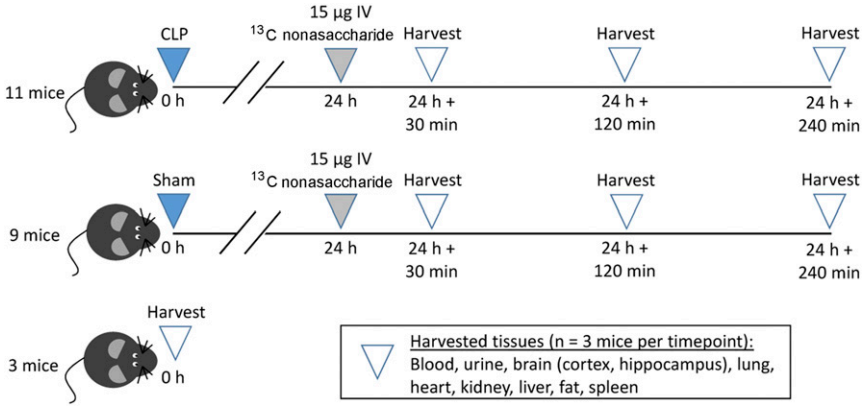

Fig. 4. Mouse study design is shown. C57BL/6 mice underwent cecal ligation and puncture (CLP) to induce sepsis or sham surgery; 24 h later (a time point characterized by peak circulating heparan sulfate), we administered ^{13}C-labeled nonasaccharide by intravenous tail vein injection. We harvested mice at various time points thereafter to determine the rate of heparan sulfate clearance. Untreated mice (control) were harvested to confirm the absence of ^{13}C-heparan sulfate oligosaccharides.

presence of microgram amounts of endogenous (^{12}C) heparan sulfate (18).

Analysis of mouse tissues (*SI Appendix*, Table S4) showed no ^{13}C-labeled nonasaccharide **11** was detectable in the control animal, confirming the expected absence of background interference in MRM analysis (Fig. 5 *B* and *C* and *SI Appendix*, Table S5). In Fig. 5*C*, the estimated concentration of ^{13}C-labeled nonasaccharide **11** in plasma right after intravenous administration is 15,000 ng/mL. In the sham plasma group, as expected the ^{13}C-labeled nonasaccharide **11** was present in the plasma 30 min after its intravenous administration, but with a rapid decrease in concentration, and then slowly cleared off within 240 min. However, in CLP plasma group, the concentration of the ^{13}C-labeled nonasaccharide **11** remained high and showed a slight delay in plasma clearance compared with sham in the first 30 min, and then cleared quickly after 30 min. In the sham urine group (Fig. 5*C*), the concentration of ^{13}C-labeled nonasaccharide **11** peaked at 30 min and then declined slowly. However, in CLP urine group, ^{13}C-labeled nonasaccharide **11** peaked at 120 min, which was consistent with the slight delay in plasma clearance. A small amount of ^{13}C-labeled nonasaccharide **11** was detected and quantified in the hippocampus samples after 30 min; this accumulation persisted for over 240 min postadministration (Fig. 5*B*). Trace amounts (>LOD but <LOQ) of ^{13}C-labeled nonasaccharide **11** were observed in other sampled organs with the exception of skeletal muscle tissue (*SI Appendix*, Tables S4 and S5).

Discussion

These findings support our hypothesis that circulating ^{13}C-labeled heparan sulfate nonasaccharides, which approximate the size of endothelial glycocalyx fragments released into the circulation of septic humans (4), are rapidly cleared from the plasma of normal hosts. Surprisingly, this clearance is only modestly delayed in septic animals—suggesting that circulating heparan sulfate may indeed serve as a valid biomarker of ongoing glycocalyx degradation in septic hosts. Rapid clearance of circulating heparan sulfate fragments occurs in septic animals despite impairment in urinary heparan sulfate clearance, suggesting that oligosaccharides may be cleared by alternative mechanisms, such as transvascular leakage into tissues. The penetration of heparan sulfate into tissues is clinically relevant, as sepsis-associated circulating heparan sulfate oligosaccharides are of sufficient size (~6–10 saccharides) and sulfation (enriched in *N*-sulfation) to bind to growth factors, potentially influencing downstream signaling processes of relevance to both organ injury onset and repair (8).

One unexpected finding was that ^{13}C-labeled heparan sulfate nonasaccharide selectively targeted and penetrated the hippocampal blood–brain barrier following sepsis, while sparing the cortex and other nonneuronal tissues (*SI Appendix*, Table S5). The blood–brain barrier represents a complex multicellular structure (consisting of brain microvascular endothelial cells with tightly apposed astrocytes and pericytes) that functions to tightly control the exchange of fluid and solutes between the vasculature and

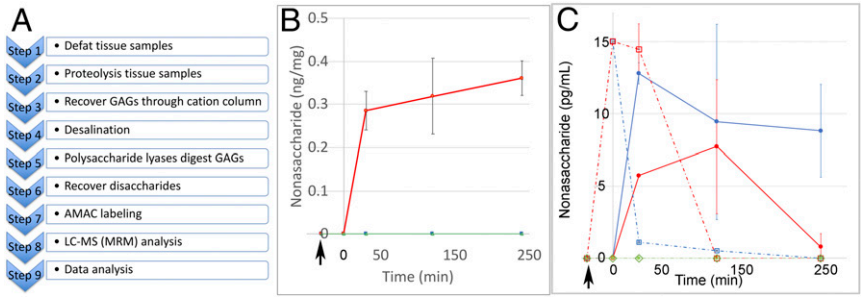

Fig. 5. LC-MS (MRM) analysis procedure and results of ^{13}C-labeled heparan sulfate nonasaccharides are shown. (*A*) GAGs recovery and LC-MS analysis flowchart for tissue samples. (*B*) The change of amount (nanograms per milligram of dry-defatted tissue) of ^{13}C-labeled nonasaccharide in hippocampus at different time points. In *B*: —■—, sham group; —●—, CLP group; and —▲—, control group. (*C*) The change in concentration (in picograms per milliliter) of ^{13}C-labeled nonasaccharide in plasma and urine at different time points. The solid line represents the following: —●—, sham urine; —●—, CLP urine; and —●—, control urine; the dashed line represents the following: -□-, sham plasma; -□-, CLP plasma; and -◇-, control plasma. The arrows indicate time of administration of ^{13}C-labeled nonasaccharide.

brain parenchyma (19). Reflecting this biological importance, numerous mechanisms regulate blood–brain barrier permeability, including lipid raft-mediated endocytosis [a process known to be influenced by heparan sulfate proteoglycans (20)] as well as receptor-mediated endocytosis [a process through which low–molecular-weight heparins are internalized by other organs (21)]. Interestingly, the hippocampal blood–brain barrier appears to be uniquely susceptible to injury, as human magnetic resonance imaging studies demonstrate a selective propensity for hippocampal (and not cortical) blood vessels to age-associated barrier dysfunction (22), as well as a tendency toward hippocampal atrophy in sepsis survivors (23). The mechanisms responsible for this selective hippocampal barrier dysfunction during sepsis, and their particular relevance to heparan sulfate extravasation, remain unknown and require future studies.

The extravasation of heparan sulfate fragments into the hippocampus may have a significant impact on BDNF-dependent hippocampal processes necessary for learning and spatial memory formation. A single intravenous dose of 15 μg of ^{13}C-labeled heparan sulfate nonasaccharide led to hippocampal concentrations of only ∼0.3 ng/mg. However, this accumulation was the consequence of only a brief period of circulating ^{13}C-heparan sulfate nonasaccharide (Fig. 5*C*), substantially underrepresenting the continuous heparan sulfate oligosaccharide shedding observed in septic mice (lasting up to 48 h) and in septic humans (at least 7 d) (8). Given that ^{13}C-heparan sulfate oligosaccharides persisted within the hippocampus (Fig. 5*B*) beyond plasma clearance (Fig. 5*C*), a continuous exposure of endogenous circulating heparan sulfate oligosaccharides would be expected to result in substantial hippocampal accumulation during sepsis. Indeed, we have recently published analytical data on plasma samples collected from septic patients enrolled in the Neurocognitive Impairment in Respiratory Failure and Shock study (8), allowing us to better understand the translational relevance of our current findings in the mouse model. Heparan sulfate in plasma collected on presentation to the hospital intensive care unit was rich in highly sulfated domains, specifically *N*- and 2-*O*-sulfo heparan sulfate. The presence of these plasma NS2S disaccharides (indeed, any disaccharides containing *N*-sulfo groups, including Tri-S) predicted the later development of moderate or severe cognitive impairment at the time of hospital discharge (or 14 d after intensive care unit discharge). Our current study confirms that oligosaccharides containing these highly sulfated domains selectively penetrate the hippocampus, where they may influence spatial memory formation by sequestering BDNF (8). Thus, therapies aimed at selectively neutralizing circulating highly sulfated heparan sulfate oligosaccharides may mitigate inhibition of hippocampal BDNF signaling, thus improving cognition. Unfortunately, a survey of known heparin-binding proteins failed to identify such a selective inhibitor (8). Future high-throughput studies are needed to identify inhibitors that may improve cognition in septic patients with minimal off-target impact on other organ systems.

Materials and Methods

General Materials and Methods. All reagents were purchased from commercial corporations. Unless noted otherwise, commercially available materials were used without further purification. Yields are given after purification, unless otherwise noted. NMR spectra were recorded on Bruker 800 spectrometer with topspin 2.1 software at 298 K. Mass data were acquired by high-resolution electrospray ionization (ESI)-MS (Thermo LTQ XL Orbitrap).

Expression of Heparan Sulfate Biosynthetic Enzymes. A total of six enzymes were used for the synthesis, including NST, C_5-epi, 2-OST, 6-OST-1, 6-OST-3, and PmHS2. All enzymes were expressed in *Escherichia coli* and purified by appropriate affinity chromatography as described previously (24).

Preparation of Enzyme Cofactors. Preparation of UDP-GlcNTFA was completed using $GlcNH_2$-1-phosphate (Sigma) and glucosamine-1-phosphate acetyltransferase/*N*-acetylglucosamine-1-phosphate uridylyltransferase (GlmU) as described previously (14, 25). Briefly, $GlcNH_2$-1-phosphate was converted to GlcNTFA using *S*-ethyl trifluorothioacetate. The resultant GlcNTFA-1-phosphate was then converted to UDP-GlcNTFA using GlmU in a buffer containing 50 mM Tris·HCl (pH 7.0), 5 mM $MgCl_2$, 200 μM DTT, 2.5 mM UTP, and 0.012 U/L inorganic pyrophosphatase. A sulfo donor, 3′-phosphoadenosine 5′-phophosulfate (PAPS), was prepared using adenosine phosphokinase and ATP-sulfurylase.

Preparation of UDP-[^{13}C]GlcA. The ^{13}C-labeled UDP-GlcA was prepared from UDP-[^{13}C]Glc (UDP-glucose) in gram scale by converting UDP-Glc to UDP-GlcA using UDP-glucose dehydrogenase (UDGH) as described previously (13). The preparation of UDP-Glc was completed by incubating fully ^{13}C-labeled glucose (from Cambridge Isotope Laboratories) using two engineered *E. coli* strains expressing four enzymes, including glucokinase (GLK), phosphoglucomutase (PGM), UDP-glucose pyrophosphorylase (UDPGP), and inorganic pyrophosphatase (PPA). [^{13}C]Glucose and UTP (from Sigma and Carbosynth, respectively) were converted to the product using the permeabilized bacterial culture to prepare UDP-Glc. It was estimated that about 8–9 g of UDP-Glc was made from the 1 L of permeabilized recombinant bacterial culture. We typically prepared 1–2 g of [^{13}C]UDP-glucose in one batch preparation. Typical reaction included 50 mM Tris, pH 7.5, 8 mM $MnCl_2$, 2 mM $MgSO_4$, 20 mM glucose, 20 mM ATP, 20 mM UTP, and permeabilized *E. coli* cells from 1-L culture. Reaction mixture was warmed to 30 °C before addition of ATP and UTP and incubated overnight with gentle shaking at 60 rpm. Completion of reaction was monitored by analytical HPLC by observing depletion of ATP and UTP peaks and appearance of UDP-[^{13}C]glucose peak. Reaction mixture was clarified by centrifugation at 9,000 × *g* to pellet the cells, and the supernatant containing the UDP glucose was collected.

To prepare UDP-[^{13}C]GlcA, the crude reaction mixture containing the UDP-glucose (∼20 mM) was pretreated with 25 mM Tris·HCl, pH 7.5, 5 mM $MgSO_4$, and 5 mM $MnCl_2$ to precipitate any cell debris that is removed by spinning at 9,000 × *g*. Typical UDP-[^{13}C]GlcA reaction contained ∼5 mM partially purified UDP-Glc, 25 mM Tris·HCl, pH 7.5, 10 mM $MgSO_4$, 0.4 mM nicotinamide adenine dinucleotide (NAD), 5 mL of crude *E. coli* lysate expressing lactic acid dehydrogenase enzyme, 40 mg of purified UDGH enzyme, and 40 mM pyruvate in 1 L. The reaction is completed in 6–8 h at 30 °C with gentle shaking at 60 rpm.

The reaction was diluted with equal volume of water and passed through Q-Sepharose (GE Life Sciences). Q columns were equilibrated with Tris·HCl pH 8.5 and eluted with buffer containing Tris·HCl pH 8.5 and 1 M NaCl. We typically obtained 0.8–1.5 g of UDP-GlcA from a batch.

General Procedure to Introduce GlcNTFA Residue for Elongation. The oligosaccharide (1.2 mmol) was incubated with PmHS2 (20 μg/mL) in buffer containing Tris (25 mmol, pH 7.2), $MnCl_2$ (15 mmol), and UDP-GlcNTFA (1.5 mmol), at room temperature overnight. The product was purified using a C18 column, and the identity was confirmed by ESI-MS (14).

General Procedure to Introduce GlcA Residue for Elongation. The oligosaccharide (1.2 mmol) was incubated with PmHS2 (20 μg/mL) in buffer containing Tris (25 mmol, pH 7.2), $MnCl_2$ (15 mmol), and UDP-GlcA (1.5 mmol) (or ^{13}C-labeled UDP-GlcA), at room temperature overnight. The product was purified using a C18 column, and the identity was confirmed by ESI-MS (14).

Procedure to Introduce *N*-Sulfate Groups on the Oligosaccharide Backbone. The oligosaccharide was suspended at 10 mg/mL in 0.1 M LiOH, and then the reaction mixture was incubated on ice for 2 h. Upon the completion of detrifluoroacetylation, the pH of the reaction mixture decreased to 7.0 and incubated with 50 mM MES (pH 7.0), 10 μg/mL NST, and 1 mM PAPS (2 equiv of oligosaccharide) at 37 °C overnight. *N*-Sulfated product was purified by Q-Sepharose (GE Healthcare), and the identity was confirmed by ESI-MS (14).

Procedure for C_5-Epimerization/2-*O*-Sulfation. The oligosaccharide was dissolved in 50 mM MES (pH 7.0), 2 mM $CaCl_2$, 10 μg/mL C_5-epi, 10 μg/mL 2-OST, and 0.2 mM PAPS (2 equiv of oligosaccharide) at 37 °C overnight. The reaction mixture was then purified by Q-Sepharose (14).

Procedure to Introduce 6-*O*-Sulfate Groups on the Oligosaccharide. The oligosaccharide was dissolved in 50 mM MES (pH 7.0), 1.5 mM PAPS (2 equiv of oligosaccharide), 0.2 mg/mL 6-OST-1, and 0.2 mg/mL 6-OST-3 in 30 mL overnight at 37 °C. The extent reaction was monitored by DEAE-HPLC to ensure the desired product reached to the highest level and the substrate was consumed (14). The reaction mixture was then purified by Q-Sepharose to obtain compound **9**.

Conversion of Undecasaccharide 9 to Nonasaccharide 11. Oligosaccharide **9** (2 mg) was dissolved in 0.4 mL of NaH_2PO_4 buffer (pH 7.0), and 20 equiv of $NaIO_4$ was added at 37 °C in the dark for 3.5 h. The reaction was quenched by the addition of ethylene glycol (20 equiv) followed by dialysis [molecular weight cutoff (MWCO), 100–500 Da] against distilled water and lyophilization. The resultant oligosaccharide (1.8 mg) was dissolved in 0.3 mL of NaH_2PO_4 buffer (pH 7.0), and then adjusted to pH 12.0 with 0.5 M NaOH aqueous. After standing at room temperature for 30 min, the solution was neutralized with 0.5 M acetic acid. The resulting mixture was dialyzed (MWCO, 100–500 Da) against distilled water and lyophilized to obtain the elimination compound **10** in 80% yield over two steps. Compound **10** (0.9 mg) was dissolved in 0.5 M TFA in 0.4-mL volume at room temperature for 24 h. The reaction was terminated by the addition of 0.5 M NaOH to pH 7.0 and dialyzed to afford 0.6-mg degradation product **11** in 85% yield.

PAGE. Phenol red dye was added to the sample for visualization of the ion front during electrophoresis. A 10-μg aliquot of each sample was analyzed on a 4–15% Mini-Protean TGX Precast Gel run in Tris-glycine buffer (at constant 30 mA for 4 h). The gel was visualized by Alcian Blue staining [0.5% (wt/vol) Alcian blue dye and 2% (vol/vol) aqueous acetic acid] and destained in water.

Experimental Procedure for Animal Study. All animal protocols were approved by the University of Colorado Institutional Animal Care and Use Committee. CLP, a model of polymicrobial peritonitis-induced sepsis, were performed on male 8- to 10-wk-old C57/BL6 mice as previously described. Briefly, mice were anesthetized with isoflurane and shaved; the mouse abdomen was prepped with chlorhexidine; and mice were administered 0.05 mg/kg s.c. buprenorphine. A midline incision was performed using a scalpel, and we externalized the mouse cecum (a blind loop of bowel, similar to the human appendix). For sham mice, we immediately reinternalized the cecum. For CLP mice, we ligated 50% of the cecum with 4:0 silk suture and then punctured the cecum through-and-through with a 22-gauge needle, creating an isolated intestinal perforation. We expressed stool using a gloved hand, and then reinternalized the cecum. For both CLP and sham mice, we reapproximated the abdominal fascia with 4:0 silk sutures and provided topical bupivacaine (1–2 mg/kg). We closed the skin with glue. We provided a second dose of buprenorphine and administered 40 μL/g saline (for fluid resuscitation) s.c. Mice recovered on a warming blanket. Twenty-four hours after CLP or sham, a time point characterized by maximal circulating heparan sulfate during murine sepsis (8, 15), we administered 15 μg of ^{13}C-labeled nonasaccharide in 100 μL of saline by tail vein injection. At various time points thereafter, mice were killed for organ harvest, with collection of plasma, urine (by direct bladder aspiration if urine was present), brain (both cortex and hippocampus), heart, lungs, liver, spleen, kidney, and mesenteric fat. Untreated mice (no CLP/sham, no ^{13}C-labeled nonasaccharide) were used as additional controls.

General Procedure for GAG Recovery and LC-MS Analysis. Tissue samples were treated with 0.5 mL of 1:1 methanol chloroform mixture for 1 h, vortexed, and dried in the hood to defat. Then the dried samples were digested by same weight amount of Actinase E (10 mg/mL) in 55 °C until all of the tissues were totally proteolyzed (36 h). GAGs were purified through Mini Q spin columns from 200 μL of the digested sample solution. GAGs eluted from Mini Q spin column were desalted by passing through a 3-kDa MWCO spin column and washed three times with distilled water. The digestion was performed in a 3-kDa MWCO spin column; 200 μL of digestion buffer (50 mM ammonium acetate containing 2 mM calcium chloride adjusted to pH 7.0) was added to the filter unit. Recombinant heparin lyase I, II, and III (pH optima 7.0–7.5) and recombinant chondroitin lyase ABC (10 mU each, pH optimum 7.4) were added to each sample and mixed well. The samples were all placed in a water bath at 37 °C overnight, after which disaccharides was collected by centrifugation. The filter unit was washed twice with 250 μL of distilled water, and the filtrates containing the disaccharide products were dried via lyophilization.

Lyophilized disaccharides were 2-aminoacridone (AMAC)-labeled by adding 10 μL of 0.1 M AMAC in dimethyl sulfate/acetic acid [17/3 (vol/vol)] incubating at room temperature for 10 min, followed by adding 10 μL of 1 M aqueous sodium cyanoborohydride and incubating for 1 h at 45 °C. The known concentration nonasaccharide standards prepared from 0.005 to 50 ng/μL were similarly digested and AMAC-labeled and used for each run as an external standard. After the AMAC-labeling reaction, the samples were centrifuged, and each supernatant was recovered and analyzed by a modification of a previously published method (26). LC was performed on an Agilent 1200 LC system at 45 °C using an Agilent Poroshell 120 ECC18 (2.7 μm, 3.0 × 30 mm) column. Mobile phase A was 50 mM ammonium acetate aqueous solution, and the mobile phase B was methanol. The mobile phase passed through the column at a flow rate of 300 μL/min. The gradient was 0–10 min, 5–45% B; 10–10.2 min, 45–100% B; 10.2–14 min, 100% B; 14–22 min, 100–5% B. Injection volume is 2 μL. A triple-quadrupole mass spectrometry system equipped with an ESI source (Thermo Fisher Scientific) was used a detector. The on-line MS analysis was at the MRM mode. MS parameters were as follows: negative ionization mode with a spray voltage of 3,000 V, a vaporizer temperature of 300 °C, and a capillary temperature of 270 °C. The data analysis was performed through Xcalibur software. The amount of ^{13}C-labeled nonasaccharides was calculated based on the amount of digested ^{13}C-labeled disaccharides.

ACKNOWLEDGMENTS. This work was supported by National Institutes of Health Grants HL125371 (to E.P.S. and R.J.L.), HL094463 (to J.L. and R.J.L.), CA231074 (to R.J.L.), GM125095 (to E.P.S. and P.S.H.), and DK111958 (to R.J.L.).

1. Liu V, et al. (2014) Hospital deaths in patients with sepsis from 2 independent cohorts. *JAMA* 312:90–92.
2. Iwashyna TJ, Ely EW, Smith DM, Langa KM (2010) Long-term cognitive impairment and functional disability among survivors of severe sepsis. *JAMA* 304:1787–1794.
3. Schmidt EP, et al. (2012) The pulmonary endothelial glycocalyx regulates neutrophil adhesion and lung injury during experimental sepsis. *Nat Med* 18:1217–1223.
4. Schmidt EP, et al. (2014) The circulating glycosaminoglycan signature of respiratory failure in critically ill adults. *J Biol Chem* 289:8194–8202.
5. Schmidt EP, et al. (2016) Urinary glycosaminoglycans predict outcomes in septic shock and acute respiratory distress syndrome. *Am J Respir Crit Care Med* 194:439–449.
6. Haeger SM, Yang Y, Schmidt EP (2016) Heparan sulfate in the developing, healthy, and injured lung. *Am J Respir Cell Mol Biol* 55:5–11.
7. Colbert JF, Schmidt EP (2016) Endothelial and microcirculatory function and dysfunction in sepsis. *Clin Chest Med* 37:263–275.
8. Hippensteel JA, et al. (2019) Circulating heparan sulfate fragments mediate septic cognitive dysfunction. *J Clin Invest* 129:1779–1784.
9. Linhardt RJ (2003) 2003 Claude S. Hudson Award address in carbohydrate chemistry. Heparin: Structure and activity. *J Med Chem* 46:2551–2564.
10. Gallagher JT, Turnbull JE, Lyon M (1992) Patterns of sulphation in heparan sulphate: Polymorphism based on a common structural theme. *Int J Biochem* 24:553–560.
11. Xu Y, et al. (2017) Synthetic oligosaccharides can replace animal-sourced low-molecular weight heparins. *Sci Transl Med* 9:5954.
12. Xu Y, et al. (2014) Homogeneous low-molecular-weight heparins with reversible anticoagulant activity. *Nat Chem Biol* 10:248–250.
13. Xu Y, et al. (2011) Chemoenzymatic synthesis of homogeneous ultralow molecular weight heparins. *Science* 334:498–501.
14. Zhang X, et al. (2017) Chemoenzymatic synthesis of unmodified heparin oligosaccharides: Cleavage of *p*-nitrophenyl glucuronide by alkaline and Smith degradation. *Org Biomol Chem* 15:1222–1227.
15. Yang Y, et al. (2017) Fibroblast growth factor signaling mediates pulmonary endothelial glycocalyx reconstitution. *Am J Respir Cell Mol Biol* 56:727–737.
16. Li G, et al. (2015) Glycosaminoglycanomics of cultured cells using a rapid and sensitive LC-MS/MS approach. *ACS Chem Biol* 10:1303–1310.
17. Sun X, et al. (2015) Analysis of total human urinary glycosaminoglycan disaccharides by liquid chromatography–tandem mass spectrometry. *Anal Chem* 87:6220–6227.
18. Warda M, et al. (2006) Isolation and characterization of heparan sulfate from various murine tissues. *Glycoconj J* 23:555–563.
19. Varatharaj A, Galea I (2017) The blood-brain barrier in systemic inflammation. *Brain Behav Immun* 60:1–12.
20. Christianson HC, Belting M (2014) Heparan sulfate proteoglycan as a cell-surface endocytosis receptor. *Matrix Biol* 35:51–55.
21. Pempe EH, Xu Y, Gopalakrishnan S, Liu J, Harris EN (2012) Probing structural selectivity of synthetic heparin binding to stabilin protein receptors. *J Biol Chem* 287: 20774–20783.
22. Montagne A, et al. (2015) Blood-brain barrier breakdown in the aging human hippocampus. *Neuron* 85:296–302.
23. Semmler A, et al. (2013) Persistent cognitive impairment, hippocampal atrophy and EEG changes in sepsis survivors. *J Neurol Neurosurg Psychiatry* 84:62–69.
24. Liu R, et al. (2010) Chemoenzymatic design of heparan sulfate oligosaccharides. *J Biol Chem* 285:34240–34249.
25. Masuko S, et al. (2012) Chemoenzymatic synthesis of uridine diphosphate-GlcNAc and uridine diphosphate-GalNAc analogs for the preparation of unnatural glycosaminoglycans. *J Org Chem* 77:1449–1456.
26. Bhattacharyya S, et al. (2018) Decline in arylsulfatase B expression increases EGFR expression by inhibiting the protein-tyrosine phosphatase SHP2 and activating JNK in prostate cells. *J Biol Chem* 293:11076–11108.